Thermodynamics of random-exchange Heisenberg antiferromagnetic chains

S. R. Bondeson and Z. G. Soos
Department of Chemistry, Princeton University, Princeton, New Jersey 08544
(Received 19 February 1980)

Diagrammatic valence-bond methods are introduced for $s = 1/2$ magnetic insulators whose random Heisenberg exchanges satisfy some distribution $f(x)$. Rapid solution of arbitrary 10-spin replicas yields, for the first time, complete static thermodynamics by generating successive replicas whose exchanges match $f(x)$. The usual singular distribution $Jx^{-\gamma}$ for structurally disordered tetracyanoquinodimethane (TCNQ) salts is contrasted with a nonsingular distribution for a random concentration c of weak exchanges ϵJ along a chain of uniform Js. A renormalization procedure for interactions among odd segments at low temperature generates a wide range of couplings for a *single* $\epsilon > 0$ and yields power laws for nonsingular $f(x)$. Experimental magnetic susceptibility $\chi(T)$, magnetization $M(T,H)$, and magnetic specific heat $C(T,H)$ results for the closely similar 1:2 complexes of quinolinium and acridinium with TCNQ are compared to $Jx^{-\gamma}$ and to interacting segments. The usual distribution has $\gamma = 0.75$ and an enormous $J = 2 \times 10^7$ K, but fails to describe the $\chi(T)$ crossover around 20 K. Interacting segments fit $\chi(T)$ over the entire range, as well as available $M(T,H)$ and $C(T,H)$ data, for some $c = 0.10$ weak exchanges $\epsilon J = 70$ K among uniform exchanges $J = 230$ K. Small differences between the two complexes were not parametrized. The microscopic picture of strong disorder leads to charge disproportionation on the TCNQ stack and to $Jx^{-\gamma}$, while weak disorder and supermolecular $TCNQ_2^-$ ion radicals rationalize the picture of weakly interacting segments.

I. INTRODUCTION

Impurities have drastic consequences in one-dimensional systems. A single vacancy, misoriented molecule, or substitutional impurity cuts the system into two segments, or interrupted strands,[1] and disrupts the transport properties.[2,3] Finite-chain effects[4] in magnetic systems produce divergent susceptibilities associated with the doubly degenerate ground state of odd-length segments. The "impurity" signal in triplet exciton crystals[5] is probably associated with misfits in dimerized chains. There are few analyses for these impurity effects, although they are known to probe the ideal, defect-free solid. Thus x-ray-generated radicals[6] were early evidence for triplet exciton motion, while substitutional doping in MnII linear chains alters both the spin dynamics[7] and the energy transport.[8] Indeed, all doping studies illustrate the uses of controlled impurities.

The low-temperature thermodynamics of the 1:2 charge-transfer complexes of quinolinium[9] (Q) and acridinium[10] (Ad) with tetracyanoquinodimethane (TCNQ) have recently been analyzed in terms of random exchanges along the one-dimensional $TCNQ^{-1/2}$ stack, thus confirming several power-law divergences discussed by Bulaevskii *et al.*[11] Modeling these systems by disordered Hubbard chains[12] or by random dimers[13] leads to rather different physical pictures.[14] The mathematical problem for either disorder or impurities involves an infinite chain of $s = \frac{1}{2}$ sites with nearest-neighbor exchange $2Jx_n$ between sites n and $n+1$. Taking parallel spins as reference and J as the unit of energy gives

$$\mathcal{H}/J = \sum_n 2x_n(\vec{s}_n \cdot \vec{s}_{n+1} - \tfrac{1}{4}) . \tag{1}$$

The antiferromagnetic exchanges $x_n \geq 0$ are random variables specified by a normalized distribution function $f(x)$. The usual choice for $f(x)$ is singular:

$$f_1(x) = (1-\gamma)x^{-\gamma}, \quad 0 \leq x \leq 1 \tag{2}$$

and contains the adjustable cutoff J at $x = 1$ and the adjustable exponent $0 < \gamma < 1$. Interacting random segments are described by

$$f_2(x) = c\delta(\epsilon - x) + (1-c)\delta(1-x) . \tag{3}$$

Here c and $1-c$ are, respectively, the concentrations of weak exchanges ϵJ and strong exchanges J along the chain.

We develop in this paper a systematic analysis of the thermodynamics of (1) for any distribution of random antiferromagnetic exchanges $f(x)$, and present explicit comparisons for $Q(TCNQ)_2$ and $Ad(TCNQ)_2$ in terms of $f_1(x)$ and $f_2(x)$. Since previous theories invoke assumed[11,12] or approximate[13,15] solutions, we both expect and find major differences.[16] Properly including the small splittings due to interactions between odd segments is particularly critical at low temperature.

The conventional picture of finite chains, or of interrupted strands, is a high-temperature approximation for noninteracting segments. For $kT \gg J$ all the spins are thermally decoupled and

none of the exchanges in (1) is important. For $kT > \epsilon J$ the exchanges J become important, but the segments are still decoupled. The conventional picture of Curie-law susceptibility divergences is the special case $\epsilon = 0$, when the odd segments remain decoupled. The more realistic picture of small, but finite, interactions between segments splits the degeneracy and suppresses Curie-law divergences. The low-temperature ($0 \lesssim kT/J \lesssim \epsilon$) thermodynamics are consequently dominated[15,4] by weak interactions among odd-length segments, and all the spins are eventually coupled for any finite interaction ϵ. Moreover, the coupling is shown in Sec. III to depend strongly on the topology of the segments. There are consequently some thermally decoupled spins at any $T > 0$. Similar conclusions apply generally to weakly coupled finite systems.

The rapid numerical solution of (1) for arbitrary 10-spin chains is the basis for all subsequent computations with the distribution functions $f_1(x)$ or $f_2(x)$. Diagrammatic valence-bond (VB) methods for $s = \frac{1}{2}$ magnetic insulators are presented in Sec. II and are derived from previous treatments of segregated[17] and mixed[18] ion-radical stacks. An effective Hamiltonian for low-temperature interactions among odd-lengths segments, as described by (3), is developed in Sec. III. The resulting thermodynamics of $f_1(x)$ and $f_2(x)$ are found in Sec. IV and are compared with experimental data on $Q(TCNQ)_2$ and $Ad(TCNQ)_2$ in Sec. V. The strong disorder associated with $f_1(x)$ and the weak disorder associated with $f_2(x)$ are contrasted in Sec. VI.

II. VB ANALYSIS OF MAGNETIC INSULATORS

Electrons are localized in magnetic insulators, but retain their spin degrees of freedom. The simplest case of one electron per site yields a spin $s = \frac{1}{2}$, with $\sigma = \alpha$ or β, and generates 2^N spin states for N sites. The following analysis of the random Heisenberg antiferromagnet (1) for finite chains can readily be generalized to other topologies or to longer-range interactions, but not to higher s. The 2^N spin states are generated by operating on a vacuum state $|0\rangle$ with an N-fold product of fermion creation operators $a^\dagger_{n\sigma}$, with $\sigma = \alpha$ or β. The restriction to a magnetic insulator guarantees that each site occurs precisely once in the N-fold product, so that the number operator satisfies

$$n_p = a^\dagger_{p\alpha} a_{p\alpha} + a^\dagger_{p\beta} a_{p\beta} = 1 , \tag{4}$$

for $p = 1, 2, \ldots, N$. This additional condition simplifies the otherwise analogous VB treatment of segregated stacks.[17]

Although each N-fold product $a^\dagger_{n\sigma}$ acting on $|0\rangle$ yields an antisymmetric, normalized eigenfunction of S_z, these functions do not diagonalize S^2. We consequently adopt operators that create or annihilate pairs of spins that are singlet or triplet correlated. The singlet generator $\theta^\dagger_{nm}$, with $n \neq m$, is

$$\theta^\dagger_{nm} = (a^\dagger_{n\alpha} a^\dagger_{m\beta} - a^\dagger_{n\beta} a^\dagger_{m\alpha})/\sqrt{2} , \tag{5}$$

$\theta^\dagger_{nm}|0\rangle$ describes a normalized singlet covalent bond between sites n and m and is represented[17] by a line connecting n and m. Any $S = 0$ VB diagram for even N entails $N/2$ applications of $\theta^\dagger_{nm}$, with each site occurring precisely once. Upon arranging the sites in a polygon, any VB diagram with intersecting lines is linearly dependent on diagrams without intersecting lines. The total number of linearly independent VB diagrams for any total S is the number N_s of representations[17] for that S. Thus $S = N/2$ occurs once, $S = N/2 - 1$ occurs $N - 1$ times, etc. The total number of singlets for even N is[19]

$$N_0 = \frac{N!}{(\frac{1}{2}N)!\,(\frac{1}{2}N+1)!} . \tag{6}$$

The dimensions of various subspaces of total S are listed in Table I. We next rewrite the spin operators in (1) in terms of the fermion operators $a^\dagger_{n\sigma}$, $a_{n\sigma}$,

$$\begin{aligned} s^+_n &= a^\dagger_{n\alpha} a_{n\beta} , \\ s^-_n &= a^\dagger_{n\beta} a_{n\alpha} , \\ 2s_{nz} &= a^\dagger_{n\alpha} a_{n\alpha} - a^\dagger_{n\beta} a_{n\beta} . \end{aligned} \tag{7}$$

It follows directly from (7) and (4) that

$$\vec{s}_n \cdot \vec{s}_m - \tfrac{1}{4} = -\theta^\dagger_{nm} \theta_{nm} , \tag{8}$$

where θ_{nm} is the adjoint of $\theta^\dagger_{nm}$. This identity holds for any $n \neq m$ and shows that isotropic exchange conserves total S, since only singlet generators occur.

Substitution of (8) into (1) shows that the operators $-2x_n \theta^\dagger_{nn+1} \theta_{nn+1}$ for $n = 1, 2, \ldots$ produce linear relations among the VB basis states. For example, sites n and $n+1$ are either connected or not

TABLE I. Number of representations N_s of total spin S for N sites with spin $s = \frac{1}{2}$.

N	$N_T = 2^N$	$S=0$	1	2	3	4	5	6
2	4	1	1					
4	16	2	3	1				
6	64	5	9	5	1			
8	256	14	28	20	7	1		
10	1024	42	90	75	35	9	1	
12	4096	132	297	275	154	54	11	1

connected to each other in any singlet VB diagram. In the former case, $\theta^\dagger_{nn+1}|0\rangle$ occurs and we have

$$-2x_n\theta^\dagger_{nn+1}\theta_{nn+1}\theta^\dagger_{nn+1}|0\rangle=-2x_n\theta^\dagger_{nn+1}|0\rangle\,. \tag{9}$$

The VB diagram is an eigenfunction with eigenvalue $-2x_n$. In the latter case, n and $n+1$ are connected to sites p and k, which are all distinct according to (4). Direct multiplication now gives

$$-2x_n\theta^\dagger_{nn+1}\theta_{nn+1}\theta^\dagger_{pn}\theta^\dagger_{n+1k}|0\rangle=x_n\theta^\dagger_{nn+1}\theta^\dagger_{pk}|0\rangle\,. \tag{10}$$

We obtain a new $S=0$ VB diagram in which sites n, $n+1$, and p,k are singlet correlated and all other sites are undisturbed. The order of the subscripts in (10) is immaterial. Operating with (1) on the N_0 linearly independent $S=0$ VB diagrams thus produces N_0 linear equations for the coefficients x_n, always with a factor of -2 on the diagonal and $+1$ elsewhere. As shown in Fig. 1, there are only two singlets for $N=4$ and operating with $\mathcal{H}/J$ in (1) yields

$$\begin{aligned}\mathcal{H}|1\rangle&=-2(x_1+x_3)|1\rangle+x_2|2\rangle\,,\\ \mathcal{H}|2\rangle&=-2x_2|2\rangle+(x_1+x_3)|1\rangle\,.\end{aligned} \tag{11}$$

The resulting unsymmetric matrix of the coefficients gives the singlet eigenvalues and the eigenfunctions as linear combinations of the VB diagrams $|1\rangle$ and $|2\rangle$. The dimensions N_0 for larger N are given in Table I and can readily be solved for arbitrary $x_1, x_2, \ldots, x_{N-1}$ in subspaces of over 10^2 VB diagrams. The eigenvalues $\lambda(p,S)$ for $p=1,2,\ldots,N_0$ and $S=0$ are measured from the absolute ground state $\lambda(1,0)$.

Since only integral S occurs for even N, we seek generators for even numbers of parallel spins. The generators for $S=1$ and 2 are, respectively,

$$\begin{aligned}\chi^\dagger_{nm}(1,1)&=a^\dagger_{n\alpha}a^\dagger_{m\alpha}|0\rangle\,,\\ \chi^\dagger_{nmpq}(2,2)&=a^\dagger_{n\alpha}a^\dagger_{m\alpha}a^\dagger_{p\alpha}a^\dagger_{q\alpha}|0\rangle\,,\end{aligned} \tag{12}$$

and are represented in Fig. 1 by VB diagrams involving an arrow from n to m or from n to m to p to q. According to (4), the $2S$ sites for a spin S are all distinct. The lowering operator S^- for these sites can be constructed from (7). The generators (12) produce the states $|SS\rangle$ with the largest S_z. The remaining $|SM\rangle$ states with $M=S-1,\ldots,-S$ are found by applying S^- to $|SS\rangle=\chi^\dagger|0\rangle$.

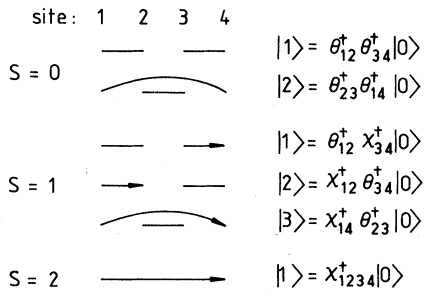

FIG. 1. Valence-bond diagrams and wave functions for a chain of four spins.

A VB diagram for $S\neq 0$ thus contains precisely one arrow connecting $2S$ sites and $\frac{1}{2}(N-2S)$ singlet-correlated pairs represented by lines. The restriction (4) to a single unpaired electron per site implies that no site index in $\theta^\dagger_{nm}$ or $\chi^\dagger_{pq}$ is repeated in any VB ket and that every site is part of a line or of the arrow. The Heisenberg exchange (1) now leads to three possibilities: (a) Sites n,m are singlet correlated, in which case (9) and (10) give the result for operating with $\theta^\dagger_{nn+1}\theta_{nn+1}$. (b) Sites $n,n+1$ have parallel spins and are both part of the arrow; now θ_{nn+1} annihilates the VB ket and there is no contribution. (c) Either n or $n+1$ is part of the arrow, while the other is not. We then find

$$\begin{aligned}-2\theta^\dagger_{nn+1}\theta_{nn+1}\chi^\dagger_{pn}\theta^\dagger_{n+1k}|0\rangle&=\theta^\dagger_{nn+1}\chi^\dagger_{pk}|0\rangle\,,\\ -2\theta^\dagger_{nn+1}\theta_{nn+1}\theta^\dagger_{pn}\chi^\dagger_{n+1k}|0\rangle&=\theta^\dagger_{nn+1}\chi^\dagger_{pk}|0\rangle\,.\end{aligned} \tag{13}$$

New VB diagrams are again produced, with sites n, $n+1$ singlet correlated. The phase relation defined by the original arrow is retained for open chains. The linear equations for the $S=1$ subspace for $N=4$ are immediately found from the VB diagrams in Fig. 1,

$$\begin{aligned}\mathcal{H}|1\rangle&=-2x_1|1\rangle+x_2|3\rangle\,,\\ \mathcal{H}|2\rangle&=-2x_3|2\rangle+x_2|3\rangle\,,\\ \mathcal{H}|3\rangle&=-2x_2|3\rangle+(x_1+x_3)|1\rangle\,.\end{aligned} \tag{14}$$

The unsymmetric matrix of the coefficients is diagonalized to obtain the eigenvalues $\lambda(p,S)$ for $p=1,2,\ldots,N_1$ and $S=1$. Explicit multiplication of the generators verifies the proper coefficients or phases, but the direct manipulation of the VB diagrams is far more rapid. The rules above work smoothly for open chains and in fact always produce $+1$ factors for off diagonal x_n.

Each N_s-dimensional subspace in Table I yields N_s roots $\lambda(p,S)$. We reference these to the absolute ground state $\lambda(1,0)$. The Zeeman interaction with a static field H is

$$\frac{\mathcal{H}_Z}{J}=h\sum_n s_{nz}\,, \tag{15}$$

where $h=g\mu_B H/J$. Since all sites have the same g value and $\mathcal{H}_Z$ commutes with (1), the energies in a field are simply

$$\lambda(p,S,M)=\lambda(p,S)+hM\,, \tag{16}$$

with $M=S,S-1,\ldots,-S$. The zero-field solution

of (1) for arbitrary x_n can immediately be generalized to $h \neq 0$. For even N, the partition function is

$$Z_N = \sum_{S=0}^{N/2} \sum_{p=1}^{N_S} \sum_{M=-S}^{S} \exp[-\beta\lambda(p,S,M)] \tag{17}$$

with $\beta = J/kT$. The $(2S+1)$-fold degeneracy for $h=0$ speeds up the numerical evaluation of (17) for fixed β, h, and x_n. Static thermodynamics[20] then involve standard derivatives of $\ln Z_N$ with respect to β and h. Derivatives are conveniently taken before carrying out the indicated sums.

The largest subspace for 10 spins has $N_1 = 90$. All eigenvalues for $N=10$ are found in a few (about 10) seconds of computer time for any input coefficients x_n in (1). The longer chain $N=12$ is still feasible, but is somewhat tedious and would not improve the analysis significantly. The efficient VB solution of any 10-spin chain allows alternate strategies for describing longer systems, as shown in the following section.

III. EFFECTIVE HAMILTONIAN FOR INTERACTING RANDOM SEGMENTS

The following analysis for interactions among odd-length segments is particularly simple for the distribution (3), which involves two energies J and ϵJ. The procedure is quite general, however, since thermal decoupling occurs whenever kT exceeds some $2x_n J$ in (1), while $kT \gg J$ leads to completely decoupled spins for any $f(x)$. The distribution function (3) describes randomly occurring weak exchanges. The probability for a segment of n sites with $n-1$ consecutive strong exchanges is simply

$$p(n) = c(1-c)^{n-1}, \quad n = 1, 2, \ldots . \tag{18}$$

It follows that $p(n)$ is normalized and that the average segment length is

$$\bar{n}(c) = \sum_{n=1} np(n) = c^{-1}. \tag{19}$$

The probabilities for even and odd segments are, respectively,

$$\begin{aligned} P_e &= \sum_{n=1} 2np(2n) = (1-c)/(2-c), \\ P_0 &= 1 - P_e = (2-c)^{-1}. \end{aligned} \tag{20}$$

The ground state of every odd segment is a doublet described by an effective spin $s = \frac{1}{2}$.

The thermodynamics of noninteracting finite segments are obtained from their exact partition functions Z_n,

$$\ln Z^{(0)} = \sum_n [p(2n) \ln Z_{2n} + p(2n-1) \ln Z_{2n-1}]. \tag{21}$$

The partition function for $N = 2n$ is given in (17), with $x_p = 1$ for $p = 1, 2, \ldots, 2n-1$. Setting $x_{2n-1} = 0$ produces an odd segment and a free spin at site $2n$. The partition function for the latter is

$$z = 1 + \exp(\beta h). \tag{22}$$

It follows that odd segments are described by

$$\ln Z_{2n-1} = \ln Z_{2n}(x_{2n-1} = 0) - \ln z. \tag{23}$$

The 10-spin result (17) is thus applicable to odd segments of up to 9 spins.

Every odd segment has a doublet ground state, which we describe by an effective spin $\frac{1}{2}$. For $\epsilon = 0$, noninteracting segments produce a Curie susceptibility for $P_0 c$ free spins per site. This follows from (21), since Z_{2n-1} reduces to z in the limit $T \to 0$. Finite ϵ lifts the degeneracies of odd segments and regains an effective Hamiltonian like (1) for the $s = \frac{1}{2}$ ground states. In order to avoid double counting the ground states of odd segments, we write the exact partition function as

$$\ln Z = \ln Z^{(0)} - P_0 \ln z + \ln Z'. \tag{24}$$

Here $P_0 \ln z$ describes the noninteracting ($\epsilon = 0$) odd segments, while Z' gives the actual splittings of order ϵ. The high-temperature result (21) is regained for $kT/J > \epsilon$, where $\ln Z'$ reduces to $P_0 \ln z$. The low-temperature behavior is described by $\ln Z'$, since for $kT/J < \epsilon$ the $P_0 \ln z$ term cancels $\ln Z^{(0)}$. Explicit illustrations for the crossover from low to high temperature are given below.

For $kT \ll J\epsilon$, we must consequently analyze the properties of random sequences of even (e) and odd (o) segments whose excited states have been frozen out. Every odd segment has an effective spin, $s = \frac{1}{2}$, while even segments behave as diamagnetic spacers. The topology of e and o segments is crucial, since intervening e segments attenuate interactions between unpaired electrons on o segments. We renormalize by computing the effective interaction x_k in (1) between odd segments k and $k+1$, which depends both on the lengths of o_k and o_{k+1} and on intervening e segments.

The effective exchanges x_k are found perturbatively for $\epsilon \ll 1$. The ground-states spin density $\rho(2n-1)$ at the terminal site controls, to first order in ϵ, the splitting of adjacent odd segments $(o_1 o_2)$. Terminal spin densities for noninteracting segments are listed in Table II and shown in Fig. 2. A simple but tedious procedure for computing ρ at any site $p = 1, 2, \ldots, 2n-1$ is to expand the VB ground state in terms of orthonormal spin functions $a^\dagger_{1\sigma} a^\dagger_{a\sigma'} \cdots a^\dagger_{2n-1\sigma''} |0\rangle$. The squares of coefficients of $a^\dagger_{p\alpha}$ and $a^\dagger_{p\beta}$ are added and subtracted, respectively, to find ρ at site p. Previous VB

TABLE II. Exact VB results for the ground-state spin density $\rho(2n-1)$ at the terminal site of odd segments, and for the attenuation $g(2n)$ for an even segment between two free spins.

n	$\rho(2n-1)$	$g(2n)$
1	1.0000	0.2500
2	0.6667	0.1890
3	0.5117	0.1564
4	0.4203	0.1352
5	0.3592	

analysis[21] for the allyl ($N=3$) radical led to spin densities of $(\frac{2}{3}, -\frac{1}{3}, \frac{2}{3})$ and was important in confirming that correlations account for negative spin densities. Open chains of $2n-1$ have symmetric spin densities about n that are negative on even sites and positive on odd sites.

The shortest possible odd segments are free spins, with $\rho(1)=1$, that produce a singlet-triplet splitting of 2ϵ. The attenuation $\rho(2n-1)$ due to longer adjacent odd segments $o_1=2n_1-1$ and $o_2=2n_2-1$ gives a first-order exchange of

$$x(o_1o_2)=\epsilon\rho(o_1)\rho(o_2) \tag{25}$$

for small ϵ. As ϵ increases, deviations from linearity are expected because the unperturbed spin densities $\rho(o_1)$ and $\rho(o_2)$ in (25) become approximate. VB methods yield the exact splitting for arbitrary ϵ in (o_1o_2) sequences of up to 10 total sites. Exact splittings for $\epsilon=0.01$, 0.10, and 0.30 are compared in Table III with the first-order result (25). The excellent agreement for small ϵ confirms the importance of terminal spin densities and justifies using (25) for (o_1o_2) sequences of over 10 sites. Indeed, the smooth behavior of $\rho(2n-1)$ as $2/(n+1)$ in Fig. 2 suggests that longer individual segments can be treated approximately.

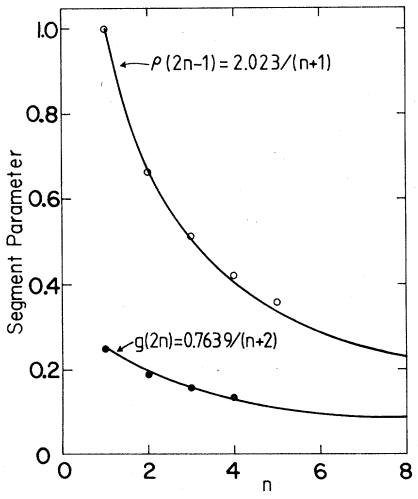

FIG. 2. Exact VB results for the spin density $\rho(2n-1)$ at the terminal site of odd segments and for the attenuation $g(2n)$ for an even segment between two free spins. The indicated curves suggest extrapolations to segments of more than 10 spins.

TABLE III. Comparison of exact splittings $\Delta E(\epsilon)/2\epsilon$, for adjacent odd segment o_1 and o_2 with the first-order result $\rho(o_1)\rho(o_2)$ in Eq. (25), for unperturbed segments.

Segments (o_1o_2)	$\rho(o_1)\rho(o_2)$ (Table II)	$\Delta E(\epsilon)/2\epsilon$ $\epsilon=0.01$	0.10	0.30
(1,1)	1.000	1.000	1.000	1.000
(1,3)	0.6666	0.6680	0.6783	0.6937
(1,5)	0.5117	0.5136	0.5288	0.5509
(1,7)	0.4203	0.4224	0.4401	0.4654
(1,9)	0.3592	0.3615	0.3805	0.4074
(3,3)	0.4444	0.4458	0.4569	0.4774
(3,5)	0.3411	0.3425	0.3543	0.3770
(3,7)	0.2802	0.2816	0.2937	0.3172
(5,5)	0.2618	0.2630	0.2740	0.2965

Singlet-triplet splittings for (o_1eo_2) sequences are quadratic in ϵ. The diamagnetic even spacer requires virtual excitations to couple the odd segments. The factors $g(2n)$ in Table II and Fig. 2 were obtained for $\epsilon=10^{-4}$. The lowest-order splitting for other (o_1eo_2) sequences go as

$$2x(o_1eo_2)=(2\epsilon)^2\rho(o_1)\rho(o_2)g(e)\,. \tag{26}$$

They can also be found exactly for any ϵ in sequences of up to 10 spins. We find (26) to be quantitative at $\epsilon=10^{-4}$, thus confirming the transferability of individual $g(2n)$ and $\rho(2n-1)$ factors. Table IV compares exact (o_1eo_2) splittings for $\epsilon=0.05$ and 0.30 with the lowest-order result (26). The good agreement and the smooth behavior of $g(2n)$ in Fig. 2 again justifies extrapolations to longer sequences and segments.

The attenuation of $2\epsilon g(e)$ in (26) for one even segment suggests that the singlet-triplet splitting for m even spacers goes as

$$2x(o_1e_1\cdots e_mo_2)=(2\epsilon)^{m+1}\rho(o_1)\rho(o_2)g(e_1)\cdots g(e_m)\,. \tag{27}$$

There are no new adjustable parameters. All $(o_1e_1e_2o_2)$, $(o_1e_1e_2e_3o_2)$, etc., sequences of up to 10 total spins can be solved exactly, and are compared in Table IV with (27). The agreement is remarkably good near $\epsilon=0$, and certainly gives the correct magnitudes even around $\epsilon=0.30$. We emphasize that the singlet-triplet splitting for the (1, 2, 2, 2, 2, 1) sequence is tiny, of the order of 8 mK for $J=200$ K, $\epsilon=0.2$, and $g(2)=4^{-1}$, and

TABLE IV. Comparison of exact splittings $\Delta E(\epsilon)/(2\epsilon)^{m+1}$, for odd segments separated by m even segments with the lowest-order result Eq. (27), for unperturbed segments.

Even spacers m	Segments $(o_1 e_1 \cdots e_m o_2)$	$\rho(o_1)\rho(o_2)g(e_1)\cdots g(e_m)$ (Table II)	$\Delta E(\epsilon)/(2\epsilon)^{m+1}$ $\epsilon=0.05$	0.30
$m=1$	$(1,2,1)^a$	0.2500	0.2690	0.3549
	(1,2,3)	0.1667	0.1783	0.2367
	(3,2,3)	0.1111	0.1181	0.1567
	(1,2,5)	0.1279	0.1366	0.1832
	(3,2,5)	0.0853	0.0905	0.1207
	(1,2,7)	0.1051	0.1122	0.1517
	$(1,4,1)^a$	0.1890	0.2105	0.3126
	(1,2,3)	0.1260	0.1389	0.2065
	(3,4,3)	0.0840	0.0916	0.1352
	(1,4,5)	0.0967	0.1062	0.1590
	$(1,6,1)^a$	0.1564	0.1786	0.2865
	(1,6,3)	0.1043	0.1173	0.1887
	$(1,8,1)^a$	0.1352	0.1575	0.2683
$m=2$	(1,2,2,1)	0.0625	0.0688	0.1089
	(1,2,2,3)	0.0417	0.0456	0.0711
	(3,2,2,3)	0.0278	0.0302	0.0463
	(1,2,2,5)	0.0320	0.0349	0.0543
	(1,2,4,1)	0.0472	0.0531	0.0927
	(1,2,4,3)	0.0315	0.0350	0.0597
	(1,4,2,3)	0.0215	0.0352	0.0602
	(1,4,4,1)	0.0357	0.0411	0.0792
	(1,2,6,1)	0.0391	0.0446	0.0831
$m=3$	(1,2,2,2,1)	0.0156	0.0176	0.0315
	(1,2,2,2,3)	0.0104	0.0116	0.0204
	(1,2,2,4,1)	0.0118	0.0135	0.0265
	(1,2,4,2,1)	0.0118	0.0134	0.0257
$m=4$	(1,2,2,2,2,1)	0.0039	0.0045	0.0090

[a] Defines $g(2n)$, for $\epsilon=10^{-4}$.

would be even smaller for smaller ϵ or longer even spaces in (27). Yet the probability of four consecutive even segments is $P_e^4 \sim 2^{-4}$, and such spacers are hardly rare.

The factors $\rho(2n-1)$ and $g(2n)$ for noninteracting segments in Table II thus accurately give, via (27), the singlet-triplet splitting of any $(o_1 e_1 \cdots e_m o_2)$ sequence for small ϵ. This defines the x_k along the sequences of odd segments and underscores the topological importance of the number of even spacers. The direct VB analysis of sequences involving 10 odd segments is then possible. The statistics of segment lengths and topologies is exact, while the magnitudes of x_k are approximate for finite ϵ. Static thermodynamical properties fortunately depend on the density of excited states, which here is controlled by the random distribution of weak exchanges, rather than the precise energy of each state. The renormalization procedure for interacting finite segments probably holds up to $\epsilon \sim 0.5$, while large ϵ would require different strategies based on 10-spin results.

IV. THERMODYNAMICS OF RANDOM ANTIFERROMAGNETIC CHAINS

The relevant static properties of $(\mathcal{H}+\mathcal{H}_Z)/J$ defined in (1) and (15) are the magnetization $M(T,H)$, the magnetic susceptibility $\chi(T)$, and the magnetic specific heat $C(T,H)$. They involve[20] derivatives of the exact partition function (24). The exact energies (16) for finite systems depend on the exchanges x_n in (1). At high temperature, phonons dominate $C(T,H)$ and there is negligible $M(T,H)$. We consequently focus on $\chi(T)$ for $kT/J > \epsilon$, where the segments are thermally decoupled and $\ln Z^{(0)}$ applies. The $h = g\mu_B H/J = 0$ limit of (17) yields sums over

$$Z_S = \sum_{p=1}^{N_S} (2S+1)\exp[-\beta\lambda(p,S)]. \tag{28}$$

Z_S describes a total spin S. The reduced susceptibility per site for an even segment of N spins is[17]

$$\frac{J\chi(\beta)}{Ng^2\mu_B^2} = \frac{\beta}{3N}\sum_{S=0}^{N/2} S(S+1)Z_S \Big/ \sum_{S=0}^{N/2} Z_S, \tag{29}$$

where $\beta = J/kT$ is the inverse of the reduced temperature. Results for noninteracting segments containing $N-1$ strong exchanges J are shown in Fig. 3, with odd segments computed according to (23). They resemble the finite-ring results of Bonner and Fisher,[22] whose $N \to \infty$ extrapolation is common to chains and rings and is the dashed line in Fig. 3. The higher $\chi(T)$ for segments reflects their smaller average exchange relative to rings, which have an extra J between sites 1 and N. The divergence of odd segments is clearly seen in Fig. 3.

The Curie susceptibility $\chi_c = g^2\mu_B^2/4kT$ is an upper bound for any $s = \frac{1}{2}$ system with antiferromagnetic coupling. The convenient phenomenological parameter[23] $\chi(T)/\chi_c$ thus represents the effective number of free spins. It also gives,[24] via the fluctuation-dissipation theorem, the sum of all spin correlations

$$\frac{\chi(T)}{\chi_c} = 1 + \sum_{nm}{}' \langle \vec{s}_n \cdot \vec{s}_m \rangle [s(s+1)]^{-1}, \tag{30}$$

where $\langle\ \rangle$ denotes a thermal average and $n = m$ is excluded from the sum. This exact result is not restricted to one-dimensional arrays, to $s = \frac{1}{2}$ sites, or to nearest-neighbor exchange. The behavior of (1) for *any* distribution $f(x)$ of antiferromagnetic exchanges can be analyzed, as shown in Fig. 4, in terms of $\chi(T)/\chi_c$. The dashed line corresponds to $\epsilon = 1$, when there are no weak exchanges in the infinite chain. The Curie law cP_0 describes noninteracting ($\epsilon = 0$) segments. For $c \sim 0.10$, the average length $\bar{n}$

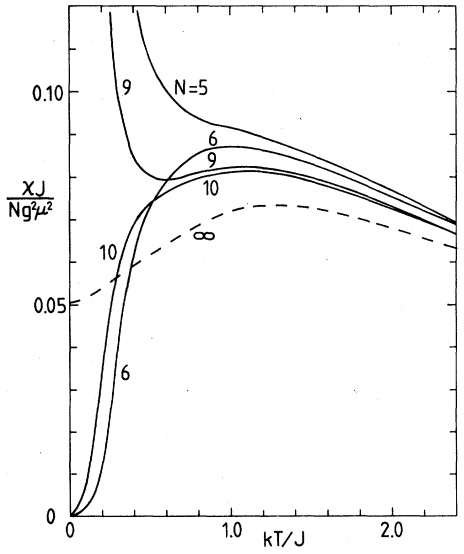

FIG. 3. Reduced susceptibility per site, Eq. (29), as a function of kT/J for noninteracting uniform segments of $N = 5$, 6, 9, and 10 spins. The dashed line is the $N \to \infty$ extrapolation from Ref. 22.

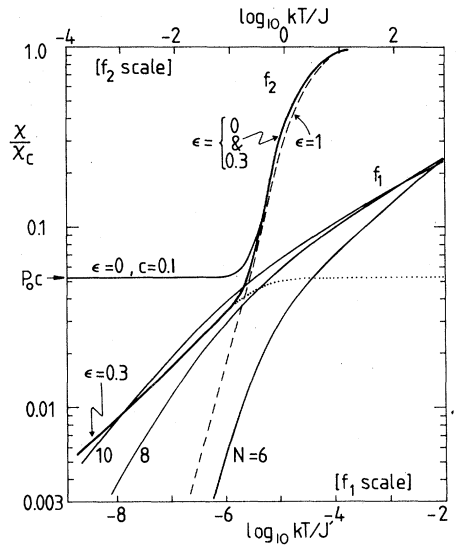

FIG. 4. The effective number of free spins $\chi(T)/\chi_c$ in Eq. (30), as a function of kT/J for the distribution $f_2(x)$ and kT/J' for $f_1(x)$. The $\epsilon = 0$, $c = 0.10$ line represents noninteracting segments of average length 10, as indicated in Eq. (31). The dashed line is the $N \to \infty$ extrapolation from Ref. 22 for uniform J. The $\epsilon = 0.30$, $c = 0.10$ curve represents 40 replicas in Eq. (33) for weakly interacting segments. The lines for $f_1(x)$ and kT/J' represent 100 replicas for $\gamma = 0.75$ and segments $N = 6$, 8, and 10 found according to Eq. (34). The dotted line is $\ln Z'$ in Eq. (24).

is about 10. The $\epsilon = 0$ curve is consequently approximated as

$$\chi^{(0)} = P_e\chi_{10} + P_o\chi_9, \tag{31}$$

where χ_9 and χ_{10} are, respectively, the susceptibilities per site of 9- and 10-spin segments in Fig. 3. Shorter segments are averaged for larger c. The approximation (31) effectively includes longer segments, which are tedious to evaluate and are close to the $N \to \infty$ extrapolation in Fig. 3. The reason is that we are neglecting both shorter segments, with larger $\chi(T)$, and longer segments, with smaller $\chi(T)$, by keeping only segments around $\bar{n} = c^{-1}$.

The $\epsilon = 0$ and 1 curves in Fig. 4 bracket the crossover from interactions between odd segments to internal excitations of thermally decoupled segments. All $\epsilon < 1$ curves must be intermediate and fall below the $\epsilon = 0$ limit of $P_0 c$ free spins per site. It follows that the nearest-neighbor exchange J dominates at high temperature for the distribution $f_2(x)$ in (3), while ϵ and c are important at low temperature. For $c \sim 0.10$, the susceptibility is given by (31) in the regime of thermally decoupled segments.

The $kT/J \ll 1$ regime is analyzed in terms of the effective interactions (27) among sequences

of 10 odd segments. The probability of three or more even spacers is $P_e^3 \sim 0.1$ for $c = 0.10$. About 10% of the effective exchanges are consequently smaller than $\epsilon^4 J$. We neglect all such exchanges and assume that they occur at every 10th site. The intervening 9 exchanges are then restricted to $(o_1 o_2)$, $(o_1 e o_2)$, or $(o_1 e_1 e_2 o_2)$. Their relative probabilities follow from (18) and are, respectively, P_o, $P_o P_e$, $P_o P_e^2$. It follows from (20) that

$$P_o + P_o P_e + P_o P_e^2 + P_e^3 = 1 . \tag{32}$$

The topological requirements of e and o segments are consequently met. Our procedure is to choose according to P_o, $P_o P_e$, $P_o P_e^2$ and then generate random numbers according to (18) to determine the o and e sequences that yield x_1 in (27). Repeating 8 times generates the x_k for the first replica, whose partition function Z_{10} in (17) is evaluated. Generating 9 more x_k according to the indicated weights produces another replica with the same *a priori* probability. For R replicas, we have

$$\ln Z = \frac{1}{R} \sum_{k=1}^{R} \ln Z_{10}^{(k)} . \tag{33}$$

The $\epsilon = 0.30$, $c = 0.10$ curve in Fig. 4 involves $R = 40$ replicas. Convergence is rapid at high T, where the average exchange counts, and slow at low T, where the lowest states of a few replicas dominate. Increasing R and comparing successive groups of 10 or 20 replicas suggests convergence to $\pm 10\%$ at the lowest T indicated in Fig. 4.

The energy gaps of order cJ for segments of length c^{-1} account for the rapid crossover around $kT/J \sim 0.1$ of the $\epsilon = 0.30$, $c = 0.10$ curve in Fig. 4. Thermally decoupled segments, as given by (31), dominate at higher T, where the intersegment interactions (the dotted line in Fig. 4) saturate at $P_0 c$ and (24) indeed reduces to $\ln Z^{(0)}$ in (21). At lower T, on the other hand, internal excitations are frozen out and (24) reduces to $\ln Z'$.

We turn next to the singular distribution $f_1(x)$ in (2), with a typical[11-13] exponent of $\gamma = 0.75$. The many resulting small exchanges allow a direct analysis of (1). For even N, we define y_1 as

$$N^{-1} = \int_0^{y_1} f_1(x)\,dx = y_1^{1-\gamma} . \tag{34}$$

It follows that N^{-1} of the exchanges satisfy $0 \leq x \leq y_1 \sim 10^{-4}$ for $N = 10$ and $\gamma = 0.75$. We neglect in (1) all exchanges $x \leq y_1$ and decouple at every Nth spin. Even N produces finite segments that ultimately become diamagnetic and spoil $T \to 0$ extrapolations. Fortunately, the interplay of o and e segments discussed in Sec. III again yields splittings that are orders of magnitude smaller than $x_1 J$, although exchanges within a segment are no longer uniform. Thus finite-chain effects are largely suppressed for a singular $f(x)$.

Now random numbers satisfying $f_1(x)$ are generated in the interval $y_1(N) \leq x \leq 1.0$. The first $N-1$ define the first N-spin replica. Each subsequent $N-1$ numbers in $y_1 \leq x \leq 1.0$ yield another replica with the same *a priori* probability. Thus (33) again holds and thermodynamic properties are simply averaged over R replicas. Convergence is slower due to the larger spread in exchanges relative to $f_2(x)$, where the large interactions are treated separately. We find $R = 100$ to be adequate for the $\chi(T)/\chi_c$ results in Fig. 4. In order to compare with kT/J results for interacting segments, the reduced temperature kT/J' refers to $f_1(x)$. The value $J' = J$ in $f_1(x)$ must be several orders of magnitude larger for comparable $\chi/\chi_c \sim 10^{-2}$.

The $N = 6$, 8, and 10 curves for $f_1(x)$ in Fig. 4 demonstrate the progressive suppression of end effects. The cutoff y_1 in (34) decreases with increasing N and, more importantly, there are better opportunities for successive diamagnetic even spacers for larger N. Thus $N = 10$ results are reliable to $\chi/\chi_c \sim 10^{-3}$. The larger $N = 12$ subspaces in Table I are within reach, should lower temperatures become important. There is no crossover in Fig. 4 for the smooth distribution function $f_1(x)$, which does not contain a dominant characteristic exchange. Instead $\chi(T)/\chi_c$ smoothly approaches unity with increasing T. Both $f_1(x)$ and $f_2(x)$ are seen to produce power laws in Fig. 4. The latter also shows a sharp crossover to thermally decoupled segments.

The direct solution of (1) for 10-spin segments, chains, or sequences thus suffices for the thermodynamics of both $f_1(x)$ and $f_2(x)$. Similar procedures can be adopted for other $f(x)$. The partition functions (17), (21), and (24) describe 10-spin replicas and must be converted to a molar basis for comparison with experiments. For example, (24) reduces to $\ln Z'$ for $kT \ll \epsilon J$ and the molar magnetization is

$$M(\beta, h) = N_A P_o c \frac{g\mu_B}{\beta} \frac{\partial}{\partial h} \ln Z' , \tag{35}$$

where N_A is Avogadro's number, $P_o c$ is the number of odd segments per site, $\beta = J/kT$, and $h = g\mu_B H/J$. The molar specific heat is

$$C(\beta, h) = k N_A P_o c \beta^2 \frac{\partial^2}{\partial \beta^2} \ln Z' . \tag{36}$$

Similar expressions apply for $f_1(x)$. We always differentiate before evaluating the sums at fixed β and h for each replica. Generating additional replicas ensures convergence, as described above for $f_1(x)$ and $f_2(x)$.

V. APPLICATION TO $Q(TCNQ)_2$ AND $Ad(TCNQ)_2$

These closely similar 1:2 TCNQ salts offer natural tests for the thermodynamics of $f_1(x)$ and $f_2(x)$. Several points should be kept in mind. First, the singular distribution $f_1(x)$ or a singular density of states was assumed in all previous work. The distribution $f_1(x)$ is shown in Fig. 5 for $\gamma = 0.75$; it has two parameters γ and J. The alternate nonsingular distribution $f_2(x)$ introduced here contains three parameters (J, ϵ, c), as shown in Fig. 5. Broadening the δ functions may eventually be justified as the precision and scope of the experimental data increases. We emphasize that $f_1(x)$ and $f_2(x)$ in Fig. 5 are quite different.

The second point is that both experimental[9-11] and theoretical[11-13] discussions have been preoccupied with the exponent γ of $f_1(x)$. Recent theory[25] demonstrates that power laws can occur without the earlier[12,13,15] requirement of a singular $f_1(x)$ or[11] of vanishing exchanges. The $f_2(x)$ results in Fig. 4 clearly show that $\chi(T)/\chi_c$ approximates a power law at low temperature. Questions about[25] possible temperature dependences of γ or about[13] differences between γ and observed powers, remain open. They become somewhat peripheral if, for example, $f_1(x)$ is inappropriate.

The final point about $Q(TCNQ)_2$ and $Ad(TCNQ)_2$ is the scatter in experimental data, as summarized in Ref. 10 for $C(T,H)$ data and in Ref. 13 for $Q(TCNQ)_2$. The pioneering Ref. 11 still has the most complete results for both complexes, but may also contain inaccuracies. The close similarities of $Q(TCNQ)_2$ and $Ad(TCNQ)_2$ results, in fact, allow the *same* theoretical parameters for both complexes, pending more detailed comparisons of experiment and theory made over wider ranges of T, P, H, etc. Such fine tuning is not attempted below. Both complexes are conveniently discussed with the same parameters in $f_1(x)$ and $f_2(x)$.

Absolute $\chi(T)$ data are shown in Fig. 6 for $Q(TCNQ)_2$ from Ref. 9(a) and for $Ad(TCNQ)_2$ from Ref. 11. The $Q(TCNQ)_2$ data in the latter are in close, but not complete, agreement. The indicated theoretical curves are from Fig. 4, with $\gamma = 0.75$ and $J = 2\times10^7$ K for $f_1(x)$ and $J = 230$ K, $\epsilon = 0.30$, and $c = 0.10$ for $f_2(x)$. The experimentally observed upturn around 20 K is readily identified as the crossover from interactions between odd segments to thermally decoupled segments. No such crossover is expected or found for $f_1(x)$. Both distributions yield power laws at low temperature, thereby confirming that a singular $f(x)$ is not required.

The inset in Fig. 6 shows that flat $\chi(T)$ behavior of both complexes at high temperature. Such behavior points to a preponderance $(90 \pm 10\%)$ of closely similar exchanges around 230 K. Since neither salt is appreciably conducting below 100 K, there is no obvious reason for postulating additional $\chi(T)$ contributions in order to retain $f_1(x)$. The proposed[12,13] corrections for exchanges around the nearest-neighbor value of J must in fact amount to something like 90% of the area under $f_1(x)$ to fit the $\chi(T)$ data. This would auto-

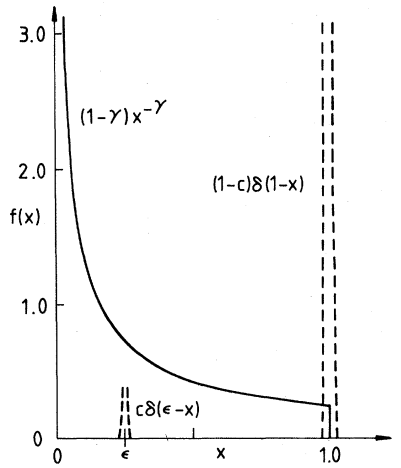

FIG. 5. Possible distributions of random exchanges. The singular distribution $f_1(x)$ in Eq. (2) has $\gamma = 0.75$; the nonsingular distribution $f_2(x)$ in Eq. (3) describes a concentration c of weak exchanges ϵJ in a chain of uniform Js.

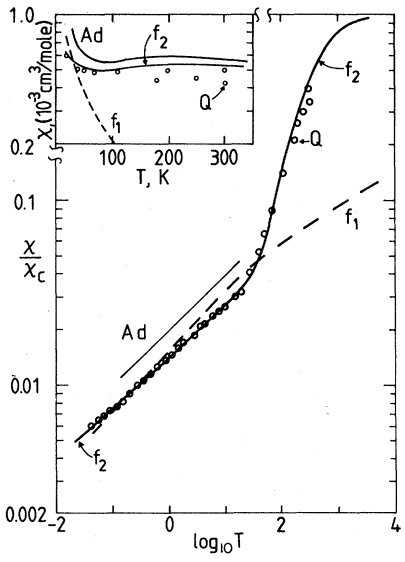

FIG. 6. Absolute $\chi(T)/\chi_c$ and (inset) $\chi(T)$ data from Ref. 9(a) for $Q(TCNQ)_2$ and from Ref. 11 for $Ad(TCNQ)_2$. The $f_2(x)$ fit for weakly interacting segments is based on $\epsilon = 0.30$, $c = 0.10$, and $J = 230$ K. The singular distribution $f_1(x)$ has $\gamma = 0.75$ and $J = 2\times10^7$ K.

matically reduce the enormous unphysical $J=2\times10^7$ K for $f_1(x)$ to a more typical[26] value of 200–300 K for organic ion-radical solids. The overall shape of $f_1(x)$ must consequently be significantly changed to match the $f_2(x)$ fit in Fig. 6, whether or not a singular distribution is retained for about 10% of weak exchanges.

The parametrization of various approximate models to $\chi(T)$ for $T<10$ K generally suffices for other static thermodynamic properties.[16] Thus the Fermi liquid choice of a singular density of states[11] and the random dimer approximation to (1) are quite comparable[13] for $Q(TCNQ)_2$. Basically, the same effective spins (30) are also responsible for $M(T,H)$ and $C(T,H)$. Since both $f_1(x)$ and $f_2(x)$ fit $\chi(T)$ below 10 K, we expect comparable fits for other properties, always using $J=230$ K, $\epsilon=0.30$, and $c=0.10$ for $f_2(x)$ and $J=2\times10^7$ K, $\gamma=0.75$ for $f_1(x)$. Additional replicas are generated when convergence is slow.

Zero-field specific-heat data are shown in Fig. 7. The $Q(TCNQ)_2$ results from Ref. 9(b) were fit to $23.6T^{0.18}$ mJ/mol K in $0.07<T<5$ K, while the $Ad(TCNQ)_2$ data from Ref. 10 gave $22.8T^{0.25}$ mJ/mol K in $0.5<T<5$ K. The lower limit can be extended as desired, while the upper bound is limited by the rapid onset of lattice contributions. An uncertainty of at least ±4 mJ/mol K is suggested by the scatter in the data. Some $R=100$ replicas were required for the $f_2(x)$ and $R=100$ were used for a rougher $f_1(x)$ fit.

TCNQ salts[26] generally have g values close to the free-electron value of 2.0023, and these complexes are not exceptions. Specifying H then

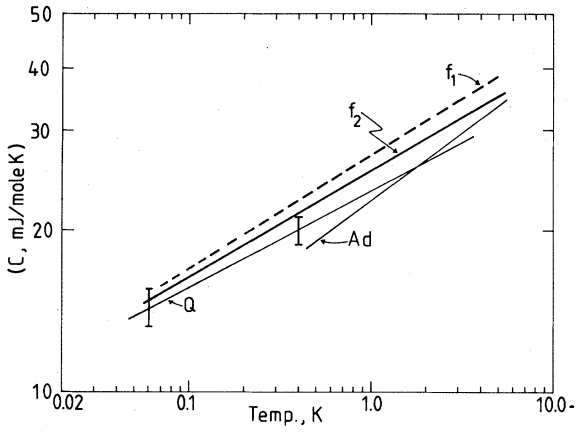

FIG. 7. Zero-field spin contributions to the molar specific heats of $Q(TCNQ)_2$ from Ref. 9(b) and of $Ad(TCNQ)_2$ from Ref. 10; the indicated lines are the quoted behavior over the observed range of T. The fits for $f_2(x)$ and $f_1(x)$ involve 100 replicas and the same model parameters as in Fig. 6.

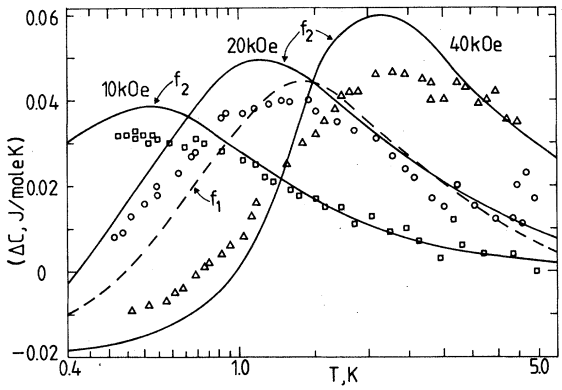

FIG. 8. Incremental magnetic specific heat $C(T,H)-C(T,O)$ in Eq. (37), for $Ad(TCNQ)_2$ from Ref. 10. The $f_2(x)$ fits for weakly interacting segments and the 20-kOe $f_1(x)$ fit again involve the model parameters from Fig. 6.

fixes $h=g\mu_BH/J$ in (16). The molar specific heat $C(T,H)$ is obtained from (36). Lattice contributions cancel[10] in

$$\Delta C(T,H)=C(T,H)-C(T,0), \tag{37}$$

as shown in Fig. 8 for $Ad(TCNQ)_2$ at $H=10$, 20, and 40 kOe and $0.5<T<5$ K, together with $f_2(x)$ and $f_1(x)$ fits. Lower temperature $Q(TCNQ)_2$ results for $C(T,H)$ from Ref. 9(b) are in Fig. 9 with $f_2(x)$ and $f_1(x)$ fits. These are the first $C(T,H)$ computations for $f_1(x)$. Previous $C(T,H)$ calculations assume random dimers[13] or a postulated Fermi liquid.[11]

The $T=0.1$ K magnetization data in Fig. 10 are from Ref. 11. The theoretical fits are based on (35). The higher value for $Ad(TCNQ)_2$ in Ref. 11 is also seen in the $\chi(T)/\chi_c$ plot in Fig. 6. This suggests a similar ~30% relative increase in $C(T,0)$, contrary to more recent work in Fig. 7. It is consequently premature to parametrize $f_2(x)$

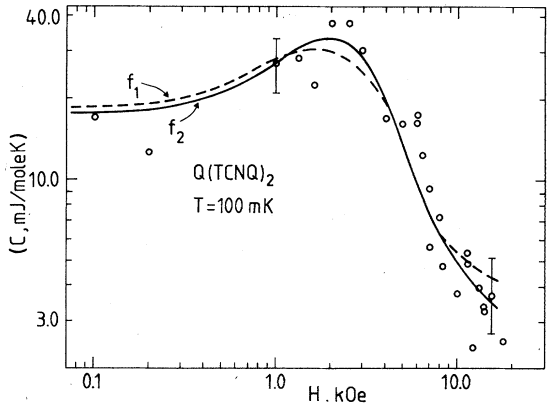

FIG. 9. Low-temperature magnetic specific heat of $Q(TCNQ)_2$ from Ref. 9(b), with $f_1(x)$ and $f_2(x)$ fits using the parameters in Fig. 6.

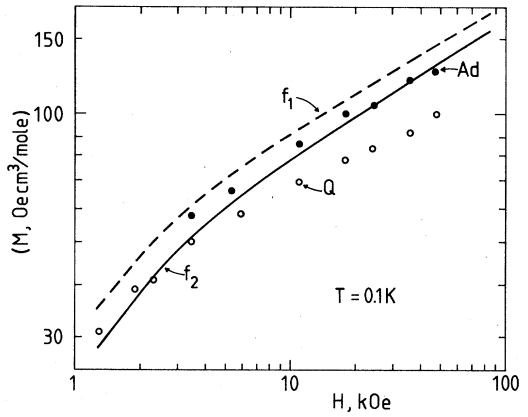

FIG. 10. Magnetization data from Ref. 11 for Q $(TCNQ)_2$ and Ad $(TCNQ)_2$, with $f_1(x)$ and $f_2(x)$ fits using the parameters in Fig. 6.

more precisely.

The choice $f_2(x)$ for weakly interacting segments thus provides an adequate description of the static thermodynamics of both $Q(TCNQ)_2$ and $Ad(TCNQ)_2$ for a concentration $c=0.10$ of weak exchanges $\epsilon J=70$ K among uniform exchanges $J=230$ K. The distribution $f_2(x)$ accounts for the crossover around 20 K in the $\chi(T)$ data, while the usual choice of $f_1(x)$ does not. The latter fits the low-temperature thermodynamics for $\gamma=0.75$ and a large J of 2×10^7 K. The direct numerical analysis of random-exchange Heisenberg antiferromagnetic chains developed above opens the way for more accurate fits based on $f_1(x)$, $f_2(x)$, or other distributions.

VI. DISCUSSION

The similar thermodynamics of other, less extensively studied TCNQ salts with asymmetric donors[27] can also be analyzed in terms of the distribution $f_1(x)$ or $f_2(x)$. As noted in the Introduction, the occurrence of chemical or mechanical defects is quite general in one-dimensional systems. The structural disorder due to asymmetric donors in many complex TCNQ is an interesting special case. There are many linear antiferromagnetic chains based on transition-metal complexes[28] and on organic ion radicals with either regular or alternating spacings.[26] The magnitudes of their "Curie tails" provides an estimate for the concentration c, of breaks in the chain, while $\chi(T)$ data at low T should fix ϵ, and reveal deviations from Curie behavior. Unless they order magnetically due to transverse interactions, we expect all one-dimensional antiferromagnets to show small but finite c and ϵ.

The prototypical disordered TCNQ salt is the 1:1 complex with N-methylphenazine (NMP), one of the earliest organic conductors.[29] The random Hubbard model[12] leading to the singular distribution $f_1(x)$ in (2) was primarily applied to NMP-TCNQ. The so far uncontrollable contamination[30] of NMP-TCNQ with $NMPH^+$ cation radicals rationalizes its variable low-temperature properties and makes it a poor choice for detailed comparison with theory. There is little doubt, however, that NMP-TCNQ yields low-temperature thermodynamics[11] that are broadly similar to those of $Q(TCNQ)_2$ or $Ad(TCNQ)_2$.

The underlying physical picture leading to random Heisenberg exchanges in TCNQ salts with disordered cations has deliberately been left open. Our goal has been to demonstrate direct VB solutions to (1) for the quite different distributions $f_1(x)$ and $f_2(x)$ in Fig. 5. As has already been noted, the $Q(TCNQ)_2$ or $Ad(TCNQ)_2$ data hardly support the exclusive use of $f_1(x)$, but leave open the possibility for many other distributions. These should have some 90% of exchanges around 230 K and some 10% weak exchanges, which need not be singular. The thermodynamics of refined versions of either $f_2(x)$ or $f_1(x)$ can also be obtained in terms of 10-spin replicas. But such numerical results are inappropriate for $T\to0$ extrapolations.

It is nevertheless interesting to contrast the underlying microscopic pictures leading to $f_1(x)$ and $f_2(x)$. The microscopic justification[12] of $f_1(x)$ in terms of random Hubbard models entails strong disorder in the TCNQ site energies, presumably due to the random orientation of the cation dipoles. When disorder dominates, favorable sites can accommodate two electrons as diamagnetic $TCNQ^{-2}$ dianions, in spite of on-site correlations U. Unfavorable sites are empty diamagnetic TCNQ molecules. Intermediate sites can accommodate one electron as $TCNQ^-$ ion radicals, but not a second on account of U. Diamagnetic A and A^{-2} sites thus break up any exchange between localized A^- spins along the TCNQ stack, except for some extra exchanges around J for adjacent A^- sites, and yield the singular distribution $f_1(x)$. We are unaware of definitive evidence for or against such strong disorder, although charge disproportionation has been ruled out in other ion-radical salts[26] and is rather unexpected.

Weak disorder is envisioned for weakly interacting segments, with an almost uniform charge density on the $TCNQ^{-0.5}$ stacks in 1:2 complexes like $Q(TCNQ)_2$ or $Ad(TCNQ)_2$. The basic unit may be an A_2^- supermolecular radical,[31] with one electron shared by two TCNQ's. There is direct EPR evidence[32] for A_2^- radicals in related 1:2 salts based on $(TCNQ)_4^{-2}$ tetramers, whose trip-

let-exciton spectra indicate half an unpaired spin on $TCNQ^{-0.5}$. No triplet-exciton splittings are expected or found in the regular $A^{-0.5}$ arrays of $Q(TCNQ)_2$ or $Ad(TCNQ)_2$. Structural disorder[33] of the cation dipole moments is again postulated to shift the TCNQ site energies, but now only enough to yield unequal sharing $A^{-(1+\delta)/2}\,A^{-(1-\delta)/2}$ within an A_2^- radical. The depleted $\frac{1}{2}(1-\delta)$ spin densities between two A_2^- radicals at unfavorable sites rationalizes a weak exchange ϵJ relative to the J for adjacent A_2^- radicals containing $A^{-0.5}$ sites. The enhanced exchange for the $\frac{1}{2}(1+\delta)$ spin densities produces no interesting effects and merely shifts the average J slightly. The result is a collection of weakly interacting segments, as described by $f_2(x)$, with uniform exchange J within segments, reduced exchange ϵJ between segments, and delocalized spin excitations within segments. There is no definitive evidence for or against this model, either.

The possibility of fitting the low-temperature thermodynamics of $Q(TCNQ)_2$ and $Ad(TCNQ)_2$ with such completely different distributions as $f_1(x)$ and $f_2(x)$ is both surprising and cautionary. While the $f_1(x)$ cutoff at 2×10^7 K is clearly unphysical, the model's main difficulty is its failure to give the observed crossover of $\chi(T)/\chi_c$ in Fig. 6. Restricted fits for several properties thus do not necessarily establish the shape of $f(x)$. Wider ranges are unfortunately often impossible due to competition from other (e.g., lattice) sources. The wide variety of physical measurements on TCNQ salts, as well as dynamic magnetic properties, should nevertheless allow discriminating between stong disorder, or $f_1(x)$ with random arrays of A, A^-, and A^{-2} sites, and weak disorder, or $f_2(x)$ and delocalized spins on weakly interacting arrays of A_2^- supermolecular radicals. The qualitative features of TCNQ salts, in general, consistently favor the latter alternative.

ACKNOWLEDGMENTS

It is a pleasure to thank Professor D. J. Klein for stimulating discussions and a thorough listing of previous numerical methods for one-dimensional spin problems. We also thank Professor W. G. Clark for access to unpublished results and discussions on $Q(TCNQ)_2$, and the National Science Foundation for financial support through NSF-DMR-7727418 A01.

[1] J. Bernasconi, D. Kuse, M. J. Rice, and H. R. Zeller, J. Phys. C 5, L127 (1972).
[2] J. Kurkijarvi, Phys. Rev. B 8, 922 (1973).
[3] V. K. S. Shante, C. M. Varma, and A. N. Bloch, Phys. Rev. B 8, 4885 (1973).
[4] R. C. Hughes and Z. G. Soos, J. Chem. Phys. 48, 1066 (1968).
[5] T. D. Buckman, O. H. Griffith, and H. M. McConnell, J. Chem. Phys. 43, 2907 (1965); D. B. Chesnut and W. D. Phillips, *ibid.* 35, 1002 (1961); I. M. Brown and M. T. Jones, *ibid.* 51, 4687 (1969).
[6] H. M. McConnell, O. H. Griffith, and D. Pooley, J. Chem. Phys. 36, 2518 (1962).
[7] D. Hone and K. G. Petzinger, Phys. Rev. B 6, 245 (1972); T. Tonegawa, J. Phys. Soc. Jpn. 47, 1471 (1979).
[8] H. Yamamoto, D. S. McClure, C. Marzzacco, and M. Waldman, Chem. Phys. 22, 78 (1977); G. L. McPherson and A. H. Francis, Phys. Rev. Lett. 41, 1681 (1978).
[9] (a) W. G. Clark, J. Hammann, J. Sanny, and L. C. Tippie, in *International Conference on Quasi One-Dimensional Conductors, Dubrovnik, Yugoslavia* (Springer, Berlin, 1979), p. 255; (b) L. J. Azevedo and W. G. Clark, Phys. Rev. B 16, 3252 (1977). See also Ref. 13.
[10] W. Duffy, Jr., F. M. Weinhaus, D. L. Strandburg, and J. F. Deck, Phys. Rev. B 20, 1164 (1979) and references therein.
[11] L. N. Bulaevskii, A. V. Zvarykina, Y. S. Karimov, R. B. Lyubovskii, and I. F. Shchegolev, Zh. Eksp. Teor. Fiz. 62, 725 (1972) [Sov. Phys.–JETP 35, 384 (1972)]; I. F. Shchegolev, Phys. Status Solidi 12, 9 (1972).
[12] G. Theodorou and M. H. Cohen, Phys. Rev. Lett. 37, 1014 (1976); G. Theodorou, Phys. Rev. B 16, 2254 (1977); 16, 2273 (1977).
[13] W. G. Clark and L. C. Tippie, Phys. Rev. B 20, 2914 (1979).
[14] Z. G. Soos, in *The Physics and Chemistry of Low-Dimensional Solids*, edited by L. Alcacer (Reidel, Dordrecht, Holland, 1980).
[15] G. Theodorou, Phys. Rev. B 16, 2264 (1977).
[16] Z. G. Soos and S. R. Bondeson, Solid State Commun. (in press).
[17] S. Mazumdar and Z. G. Soos, Synth. Metals 1, 77 (1979); S. R. Bondeson and Z. G. Soos, J. Chem. Phys. 71, 3807 (1979).
[18] Z. G. Soos and S. Mazumdar, Phys. Rev. B 18, 1991 (1978).
[19] G. Rumer, Göttingen Nachr. 1932, 377.
[20] D. C. Mattis, *The Theory of Magnetism* (Harper and Row, New York, 1965), pp. 223–229; B. C. Gerstein, in *Low-Dimensional Cooperative Phenomena*, edited by H. J. Keller (Plenum, New York, 1975), p. 131.
[21] H. M. McConnell and D. B. Chesnut, J. Chem. Phys. 28, 107 (1958); A. Carrington, Q. Rev. 17, 67 (1963).
[22] J. C. Bonner and M. E. Fisher, Phys. Rev. 135, 640 (1964).
[23] Z. G. Soos, J. Chem. Phys. 46, 4284 (1967); K. T. McGregor and Z. G. Soos, Inorg. Chem. 15, 2159 (1976).

[24]Z. G. Soos, T. T. P. Cheung, and K. T. McGregor, Chem. Phys. Lett. 46, 600 (1977).
[25]S. K. Ma, C. Dasgupta, and C. K. Hu, Phys. Rev. Lett. 43, 1434 (1979); J. E. Hirsch and J. V. José, J. Phys. C 13, L53 (1980).
[26]Z. G. Soos and D. J. Klein, in *Molecular Association*, edited by R. Foster (Academic, New York, 1975), Vol. I, pp. 1–119; Z. G. Soos, Annu. Rev. Phys. Chem. 25, 121 (1974), and references therein.
[27]G. Grüner, A. Jánossy, K. Holczer, and G. Mihály, in *International Conference on Quasi-One-Dimensional Conductors, Dubrovnik, Yugoslavia* (Springer, Berlin, 1979), p. 246; T. Kondow, U. Mizutani, and T. B. Massalki, Phys. Status Solidi 81, 157 (1977); P. Delhaes, G. Keryer, S. Flandrois, and J. P. Manceau, *ibid.* 80, 125 (1977).
[28]L. S. DeJongh and A. R. Miedema, Adv. Phys. 23, 1 (1974).
[29]L. R. Melby, Can. J. Chem. 43, 1148 (1965).
[30]H. J. Keller, D. Nöthe, W. Moroni, and Z. G. Soos, J. Chem. Soc. Chem. Commun. 1978, 331; D. Sandman, Mol. Cryst. Liq. Cryst. 50, 235 (1979).
[31]D. B. Chesnut and P. Arthur, Jr., J. Chem. Phys. 36, 2969 (1962).
[32]A. J. Silverstein and Z. G. Soos, Chem. Phys. Lett. 39, 525 (1976).
[33]H. Kobayashi, F. Marumo, and Y. Saito, Acta Cryst. Sec. B 27, 373 (1971); H. Kobayashi, Bull. Chem. Soc. Jpn. 47, 1346 (1974).